



Comparative analysis of metasurface array-based solar absorber for visible region

Jaymit Surve¹ · Juveriya Parmar^{2,4} · Shobhit K. Patel^{3,4}  · Rajendrasinh Jadeja¹

Received: 25 August 2021 / Accepted: 30 October 2021 / Published online: 8 November 2021
© The Author(s), under exclusive licence to Springer Science+Business Media, LLC, part of Springer Nature 2021

Abstract

We have proposed a graphene-based metasurface solar absorber for broadband visible wavelength range. The absorption analysis for four different designs is represented. We have explored the Four C-shape array metasurface absorber design, Five circle array metasurface absorber design, Five C-shape array metasurface absorber design, and the Four circle array metasurface absorber design for ultraviolet, visible, and infrared regions with the wavelength ranging from 0.2 to 0.8 μm . The highest average absorption is achieved for the four C-shape array metasurface absorber design. Furthermore, the absorptance response is also explored for various parameter variations such as substrate thickness, resonator thickness, and graphene chemical potential. The substrate height and resonator height have a marginal effect on absorptance. We have also analysed the design by placing graphene material spacer between gold layer and SiO_2 substrate layer. While the effect of graphene chemical potential on absorptance is negligible for 0.1–0.7 eV, but for graphene chemical potential of 0.9 eV, the absorptance plot shows a sudden decrease at around 0.69 μm wavelength. The proposed metasurface solar absorber can be applied for photovoltaic applications and solar energy harvesting applications.

Keywords Solar absorber · Metasurface · Graphene · Efficient

1 Introduction

Optical metamaterials are attracting a lot of attention due to their potential applications in photonics. The metamaterials can be engineered to obtain the expected optical characteristics by characterizing the electromagnetic properties of the material. The extensive function of optical metamaterials (MMs) has pushed research in the area of electromagnetic

✉ Shobhit K. Patel
shobhitkumar.patel@marwadieducation.edu.in

¹ Electrical Engineering Department, Marwadi University, Rajkot, Gujarat, India

² Physics Department, Marwadi University, Rajkot, Gujarat, India

³ Computer Engineering Department, Marwadi University, Rajkot, Gujarat, India

⁴ Electronics and Communication Engineering Department, Marwadi University, Rajkot, Gujarat, India

absorbers. (Freise 2012) Electromagnetic metamaterials are artificially constructed substance with exotic electromagnetic properties like negative permittivity, negative permeability (Shelby et al. 2001)–(Smith et al. 2000), and have piqued interest in various real-time applications like solar thermo-photovoltaic device (Lenert et al. 2014), sensing (Taya 2015a)–(Patel and Parmar 2021), and other optical structure designs (Li et al. 2016). Resonant absorbers, which are frequency sensitive and give absorption at resonant frequencies, and broadband absorbers, which provide absorption over a wide frequency range, are the two types of electromagnetic absorbers (Watts et al. 2012). A while ago, a ‘perfect’ absorber with near-unity absorption has been shown to be capable of producing using metamaterial which was initially postulated by Landy et al. (Landy et al. 2008). Rhee et al. reviewed multiple metamaterial-based perfect absorbers. Metamaterial-based perfect absorbers (MMPA) are applied as perfect absorber-based novel applications. MMPA is typically made up with three layers. The layer is used to prevent incident electromagnetic waves from being reflected. The middle layer is a dielectric layer that provides room for electromagnetic waves to disperse plus can also act as a resonance cavity to extend the duration that electromagnetic waves spend inside the middle layer. Finally, a continuous metallic plate blocks leftover transmission in the third layer (Rhee et al. 2014).

Metamaterial based sensors are also widely known for their applications in several fields i.e., industrial, environmental, and medical etc. (Liu et al. 2017)–(Shetti et al. 2019). Optical sensors (Ahmadivand et al. 2020; Chou et al. 2017), electrochemical sensors (Yu and Yi 2007), and physical sensors (Son et al. 2017) are the most well-known metamaterial based sensors. Optical sensors are area-of-interest for most of the researchers due to its compact size, low-cost and utilization of remarkable nanomaterials which make them easy to fabricate (Shi et al. 2017). Direct type sensors are globally utilized due to its low-cost and applications in medical domain to detect several biomolecules such as hemoglobin, urine, protein etc. (Gerislioglu et al. 2020)–(Ertürk et al. 2016). Graphene-peptide based sensor can also be used for the environmental analysis and graphene-based leaky-wave optical sensors can be used for detecting hemoglobin biomolecules (Wang et al. 2017; Patel et al. 2020a). Sensors fabricated using the gold-nanoribbons based substrate can be utilized for biomedical diagnosis for which various combination of Raman signals are recently used (Zhao et al. 2019). Taya presented a anisotropic metamaterial based waveguide sensor as an optical sensor for the applications in the domain of refractometry (Taya 2015b, 2018). S.A. Taya also investigated the dispersion properties of an anisotropic left-handed material-based waveguide identifying some of the remarkable features, i.e. presence of fundamental mode in a narrow frequency range, positive group velocity that increases with the increment in frequency, and an effective dependence of dispersion curves on the anisotropy (Taya 2015c).

Many other metamaterial structures have since been suggested in various frequency regimes, including microwave (Bhattacharyya et al. 2015; Charola et al. 2021a), terahertz (Gao et al. 2015), infrared (Feng et al. 2014; Ahir et al. 2019; Parmar and Patel 2021), and visible. However, they have low bandwidth because of one absorption point. For the forthcoming growth of physics and photonics, graphene is a swiftly rising star. Given the brief history of graphene, this essentially two-dimensional substance has remarkable crystal and electrical quality and has already unveiled a great deal of new physics and prospective utilization. Graphene, in general, is a completely new group of matters that are only one atom thick, and as such, it helps to achieve breakthroughs into low-magnitude physics, which has amazed and continues to give fertile ground for several utilities (Geim and Novoselov 2007). Graphene has magnificent electro-optical characteristics which can be applied with metasurface absorbers. Graphene also possesses exceptional optical, thermal,

and mechanical properties. Each layer of graphene with a reflectivity of less than 0.1% absorbs up to 2.3% of white light, according to research. As a result, the pure single graphene sheet has a high degree of transparency and flexibility. El-Amassi et al. explored a reflectance analysis for a symmetric parallel-plate waveguide designed by placing two graphene sheets and they observed no effect of graphene conductivity on the reflectance for high frequencies (El-Amassi and Taya 2017). Al-Ashi and co-authors presented an optical sensor designed via graphene layer surrounding an optical fiber and the maximum sensitivity was determined while decreasing the graphene conductivity (Al-Ashi et al. 2020).

Many researchers have put up significant effort to enhance bandwidth. Shen et al. (Shen et al. 2015), for example, devised a resistive film absorber that achieves near unity absorption above 90% in the frequency region of 3.9 to 26.2 GHz. Broadband absorbers are designed using metamaterials to absorb more energy and perfect absorption. Due to its perfect absorption metasurface has showcased a great promise in various fields (Cheng et al. 2012; Guo et al. 2016). A plasmonic metamaterial based on Au/SiO₂ nanocomposite absorber with a broadband visible regime of frequency. Parmar et al. presented a 'gold metasurface-based broadband near-infrared and near-visible solar absorber, which achieved 78% average absorption in the frequency region of 300–500 THz (Parmar et al. 2020). This was designed by placing square shape gold resonator over MgF₂ substrate followed by tungsten base. Wang et al. designed a graphene-based absorber in the terahertz regime. They achieved dual near unity absorption at two different frequencies (Wang et al. 2018). This design includes a cyclic pattern graphene disk followed by a gold material as a ground plane. Min Zhong presented a metamaterial-based absorber with a metal-dielectric layer design which achieves a 92% absorption peak at 4.2 THz. The absorption amplitude is improved by placing the sample in the different liquid layers of acetonitrile, acetone, methanol, or benzene and the achieved absorption amplitude for the respective liquid layer was 97%, 98%, 99%, and 99.4% (Zhong 2020).

In this paper, we have presented a high absorption metasurface-based solar absorber which is a basic requirement. The absorptance analysis is explored for four various metasurface-based absorber designs. The proposed metasurface-based solar absorber can be used as a basic element for energy harvesting devices in visible range due to its efficient, high-absorption, broadband in visible range like features. The effect of various geometrical and chemical parameters on absorptance is presented. The design modeling, metasurface absorber design results, and the conclusion are presented in section-2, section-3, section-4, respectively.

2 Design and modeling

The metasurface-based solar absorber designs are presented in Fig. 1. The first metasurface is designed by placing four C-shape array of gold resonators over a graphene spacer which is placed over a SiO₂ substrate (Four C-shape array metasurface absorber design). The second metasurface solar absorber is created by placing five circle array of gold resonator over the same graphene spacer which is situated over a SiO₂ substrate (Five circle array metasurface absorber design). The third metasurface is quite similar to the first one, the only difference is instead of four C-shape array here we are placing five C-shape array over graphene spacer. The fourth and the final metasurface solar absorber design is also identical to the second design the only variation is in the resonator pattern. Here we have placed four circle array over a graphene spacer. instead of five which was the case in the second

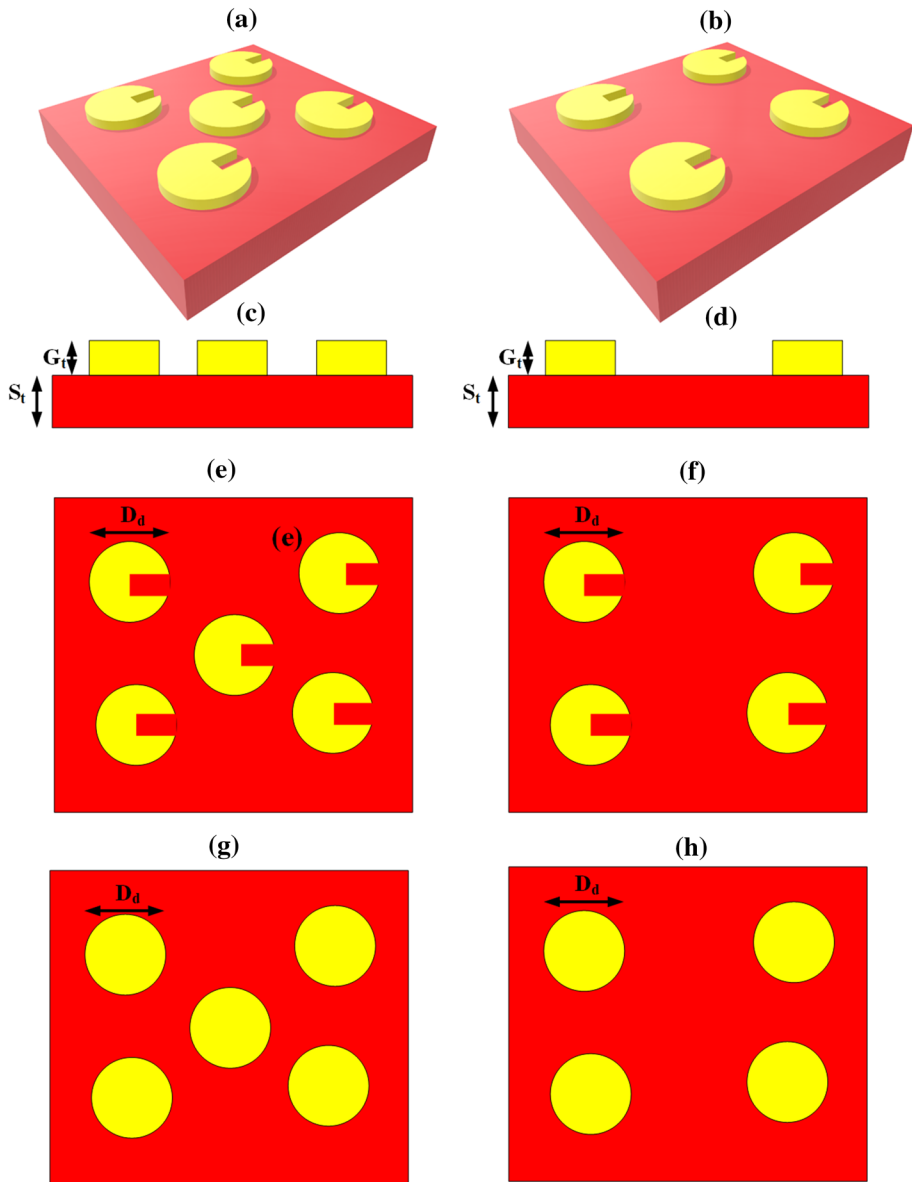


Fig. 1 Metasurface based solar absorber design **a** and **b** 3D view, **c** and **d** side view, **e–h** top view. The designs are made with gold and SiO_2 material with graphene spacer. The dimensions are: $L=20\ \mu\text{m}$, $S_h=4\ \mu\text{m}$, $r_h=1.8\ \mu\text{m}$, $D_d=6.4\ \mu\text{m}$. Light is falling on the top of the metasurface as shown in the diagram. The dimensions in the diagram are not up to the scale

design. The rest of the dimensions are the same for all designs. The various dimensions are: Length of structure $L=20\ \mu\text{m}$, Radius of the circle $R_r=3.2\ \mu\text{m}$, substrate (SiO_2) thickness $S_h=4\ \mu\text{m}$, Gold resonator thickness $r_h=1\ \mu\text{m}$. The absorption analysis for the present metasurface designs is presented here.

The graphene conductivity σ_s , derived from Eqs. (1), (2), (3) and (4) (Hanson 2008).

$$\epsilon(\omega) = 1 + \frac{\sigma_s}{\epsilon_0 \omega \nabla} \tag{1}$$

$$\sigma_{intra} = \frac{-je^2 k_B T}{\pi \hbar^2 (\omega - j2\Gamma)} \left(\frac{\mu_c}{k_B T} + 2 \ln \left(e^{\frac{\mu_c}{k_B T}} + 1 \right) \right) \tag{2}$$

$$\sigma_{inter} = \frac{-je^2}{4\pi \hbar} \ln \left(\frac{2|\mu_c| - (\omega - j2\Gamma)\hbar}{2|\mu_c| + (\omega - j2\Gamma)\hbar} \right) \tag{3}$$

$$\sigma_s = \sigma_{intra} + \sigma_{inter} \tag{4}$$

where various parameters are interpreted as, ϵ_0 is the vacuum permittivity, σ_s is the conductivity, ∇ is the thickness of graphene layer, e is the electron charge, ω is the angular frequency, k_B is the Boltzmann’s constant, \hbar is the reduced Planck’s constant, Γ is the scattering rate, σ_{intra} is the intraband conductivity and σ_{inter} is the interband conductivity, and T is the normal room temperature.

The optical conductivity of graphene is regulated by varying its chemical potential (0.1–0.9 eV). The chemical potential of graphene is calculated using $\mu_c = \hbar v_F \sqrt{\pi C V_{DC}}/e$, where V_{DC} is the gate voltage, and the capacitance is defined as $C = \epsilon_d \epsilon_0 / t$, where ϵ_d is the static permittivity and t is the thickness of the dielectric layer.

The absorptance of the absorber depends on the graphene’s conductivity (σ) and angle of incidence (θ_i) (Patel et al. 2021).

$$r(\omega, \theta_i) = \frac{\omega \cos \theta_i \prod_{00}(\omega, \theta_i)}{2i\hbar ck^2 + \omega \cos \theta_i \prod_{00}(\omega, \theta_i)} \tag{5}$$

$$\sigma_{||}(\omega, k) = -i \frac{\omega}{4\pi \hbar k^2} \prod_{00}(\omega, k) \tag{6}$$

$$r(\omega, \theta_i) = \frac{2\pi \cos \theta_i \sigma_{||}(\omega, k)}{c + 2\pi \cos \theta_i \sigma_{||}(\omega, k)} \tag{7}$$

$$\mathcal{R}(\omega, \theta_i) = |r(\omega, \theta_i)|^2 \tag{8}$$

$$\mathcal{R}(\omega, \theta_i) = \frac{4\pi^2 \cos^2 \theta_i [\text{Re}^2 \sigma_{||}(\omega, k) + \text{Im}^2 \sigma_{||}(\omega, k)]}{[c + 2\pi \cos \theta_i \text{Re} \sigma_{||}(\omega, k)]^2 + 4\pi^2 \cos^2 \theta_i \text{Im}^2 \sigma_{||}(\omega, k)} \tag{9}$$

$$\mathcal{R}(\omega) = \mathcal{R}(\omega, 0) = \frac{4\pi^2 [\text{Re}^2 \sigma(\omega) + \text{Im}^2 \sigma(\omega)]}{[c + 2\pi \text{Re} \sigma(\omega)]^2 + 4\pi^2 \text{Im}^2 \sigma(\omega)} \tag{10}$$

$$A(\omega) = 1 - \mathcal{R}(\omega) - T(\omega) \tag{11}$$

If we consider the transmittance near to zero value then absorption depends only on the reflectance values as shown below.

$$A(\omega) = 1 - \mathcal{R}(\omega) \quad (12)$$

Here, k is the wave vector.

3 Metasurface absorber designs result

The designs represented in Fig. 1 are explored for absorptance analysis and obtained results are illustrated in Figs. 2, 3, 4, 5, 6, 7, 8, 9, 10, 11, 12, 13 and 14. The Fig. 1 designs are simulated using the COMSOL Multiphysics tool with the help of the finite element method (FEM). The designs were simulated under the following condition: tetrahedral Delaunay tessellation condition with a minimum, and maximum meshing size set as 0.03 and 0.7 μm , respectively. The growth rate for meshing is set as 1.35. Furthermore, periodic boundary conditions are utilized. The results in terms of absorptance are illustrated in Fig. 2. The obtained results are also analyzed for different wavelength ranges including ultraviolet, visible, and infrared, and formatted in the table form as shown in Table 1. Among the simulated four designs, the four C-shape array metasurface absorber design is giving excellent absorptance results. The highest absorptance is achieved in the visible region with 92% of average absorptance. While the rest of the designs are giving moderate results. The results are presented in decreasing order considering their performance in Table 1. From Table 1, we can clearly say that all the four proposed designs are performing better than the mentioned reference designs. The proposed designs are performing excellently in terms of absorptance as it is achieving better absorptance in visible regime.

The designs are also simulated by varying different geometrical parameters such as substrate (SiO_2) thickness, resonator thickness, and various graphene chemical potential (GCP). The results are obtained for 0.2–0.8 μm wavelength range. The graphene layer chemical potential is varied from 0.1 to 0.9 eV and the corresponding results are presented in Figs. 3, 6, 9, and 12. The results illustrate that for the values between 0.1 and 0.7 eV there is not much discrepancy with respect to graphene chemical potential, but for the GCP of 0.9 eV, we can observe the sudden decrease in absorptance after the wavelength of 0.7 μm . The absorptance analysis is carried out for different resonator thickness values ranging from 1 μm to 1.8 μm in the step of 0.2 μm and the respective results are represented in Figs. 4, 7, 10, and 13. For four C-shape array metasurface design, the maximum absorptance of 0.991 is achieved at 0.49 μm wavelength for resonator thickness of 1.8 μm . For five circle array metasurface design, the maximum absorptance of 0.993 is achieved at 0.49 μm wavelength for resonator thickness of 1.6 μm . For five C-shape array metasurface design, the maximum absorptance of 0.991 is achieved at 0.49 μm wavelength for resonator thickness of 1.6 μm . For four circle array metasurface design, the maximum absorptance of 0.994 is achieved at 0.49 μm wavelength for resonator thickness of 1.6 μm . The results indicate that the absorptance is highest in the wavelength ranging from 0.4 to 0.7 μm and the resonator thickness does not have a very high effect on the absorptance results. We have also analyzed the effect of varying the substrate (SiO_2) thickness. For this, we have varied the substrate thickness in the range of 4 μm to 6 μm with the step of 0.5 μm and the related results are illustrated in Figs. 5, 8, 11, and 14. For four C-shape array metasurface design, the maximum absorptance of 0.993 is achieved at 0.49 μm wavelength for SiO_2 thickness of 4 μm . For five circle array metasurface design, the maximum

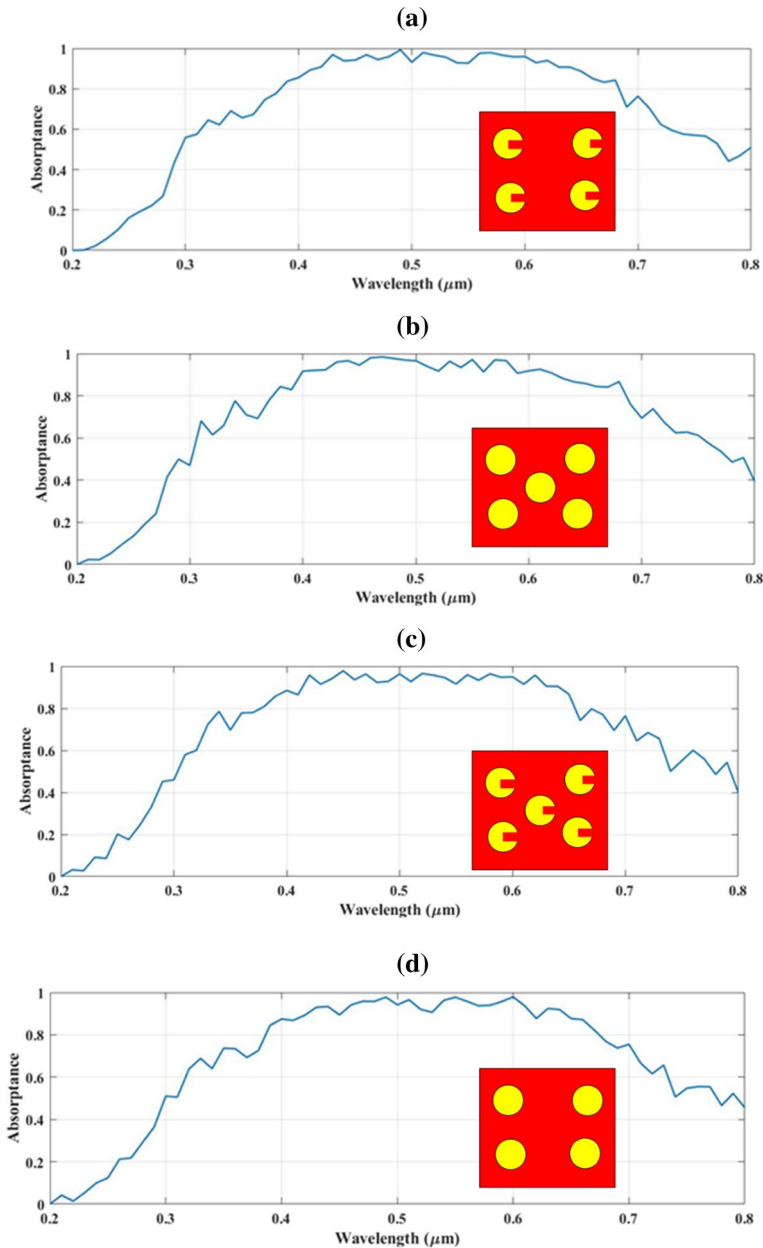


Fig. 2 Absorbance plot for **a** Four C-shape array metasurface absorber design; **b** Five circle array metasurface absorber design; **c** Five C-shape array metasurface absorber design; **d** Four circle array metasurface absorber design

absorbance of 0.99 is achieved at 0.49 μm wavelength for SiO_2 thickness of 5.5 μm . For five C-shape array metasurface design, the maximum absorbance of 0.994 is achieved at 0.49 μm wavelength for SiO_2 thickness of 4.5 μm . For four circle array metasurface design,

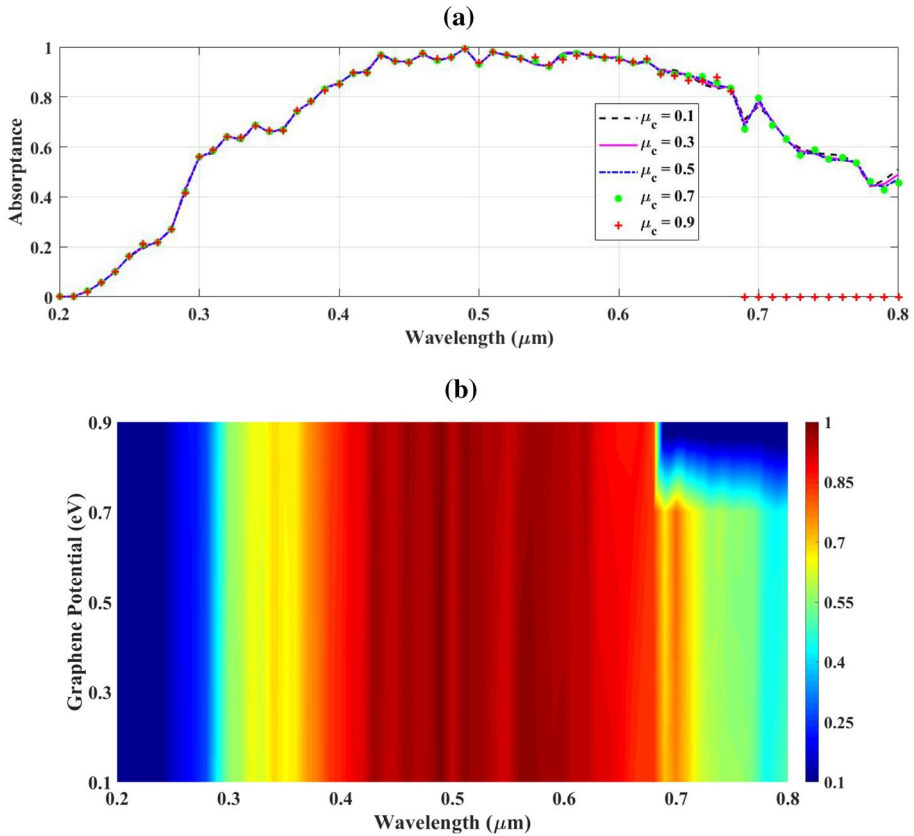


Fig. 3 Absorbance plot for various graphene potential 0.1–0.9 eV for four C-shape array metasurface design. **a** The line plot represents the absorbance for various values of GCP. The maximum absorbance of 0.993 is achieved at 0.49 μm for all graphene chemical potential values. **b** The plot illustrates that for the values between 0.1 and 0.7 eV there is not much discrepancy with respect to graphene chemical potential, but for the GCP of 0.9 eV we can observe the sudden decrease in absorbance after the wavelength of 0.69 μm . The results are obtained for 0.2–0.8 μm

the maximum absorbance of 0.993 is achieved at 0.49 μm wavelength for SiO_2 thickness of 4.5 μm . The results indicate that the maximum absorbance is achieved in the visible range which is from 0.4 to 0.7 μm . It is also clear that by varying substrate (SiO_2) thickness absorbance is not very much affected.

4 Conclusion

To conclude, a metasurface solar absorber with the help of sandwiched graphene monolayer sheet in between SiO_2 substrate and gold resonator explored for 0.2–0.8 μm wavelength range. The results of these four variations in metasurface has been compared in

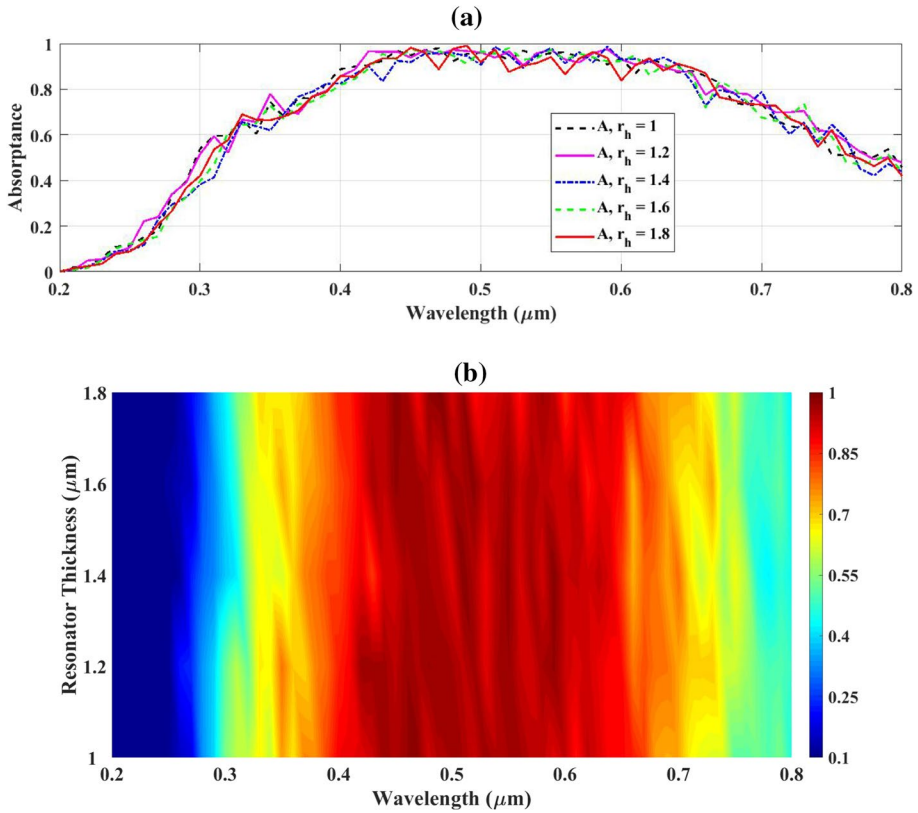


Fig. 4 Absorbance plot for various values of resonator thickness 1–1.8 μm with the increase in the step of 0.2 μm for four C-shape array metasurface design. **a** The line plot represents the absorbance for different values of resonator thickness. The maximum absorbance of 0.991 is achieved at 0.49 μm wavelength for resonator thickness of 1.8 μm . **b** The plot illustrates that the absorbance is highest for 0.4–0.7 μm range. The results are obtained for 0.2–0.8 μm range

terms of absorbance response and the best design of four C-shape array metasurface solar absorber has been identified due to achieved highest average absorbance of 92% in visible regime. The design results comparison with other published designs also show that our design has highest average absorption for the visible region. We are also gaining near unity (99.4%) absorption at 0.49 μm wavelength. Furthermore, to identify the optimized physical parameters, we have varied several geometrical parameters such as substrate thickness, and resonator thickness, clearly stating that the highest absorption is achieved for substrate thickness of 4 μm and resonator thickness of 1.8 μm . Thus the parameters have been optimized at which the highest absorbance for four C-shape array metasurface solar absorber design has been achieved. The proposed solar absorber design can also be utilized as an elementary block for an energy harvesting device in visible regime due to its high efficiency, broadband in visible like qualities.

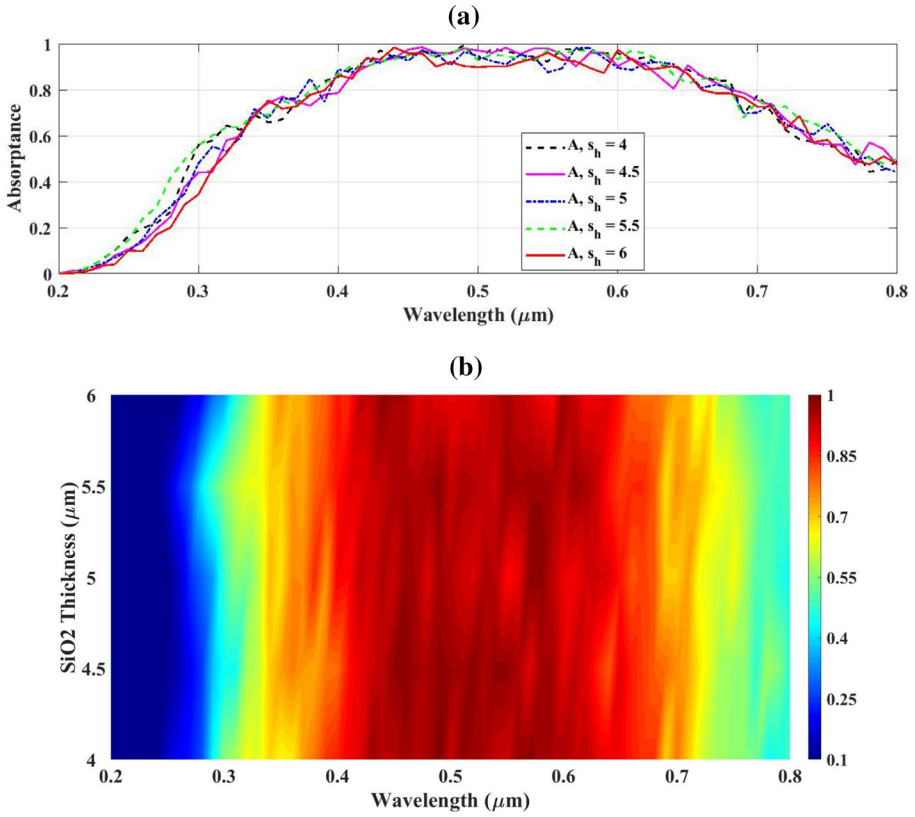


Fig. 5 Absorbance plot for various values of SiO₂ thickness in the range of 4–6 μm with the increase in the step of 0.5 μm for four C-shape array metasurface design. **a** The line plot represents the absorbance for different values of SiO₂ thickness. The maximum absorbance of 0.993 is achieved at 0.49 μm wavelength for SiO₂ thickness of 4 μm . **b** The plot illustrates that the absorbance is highest for 0.4–0.7 μm range. The results are obtained for 0.2–0.8 μm range

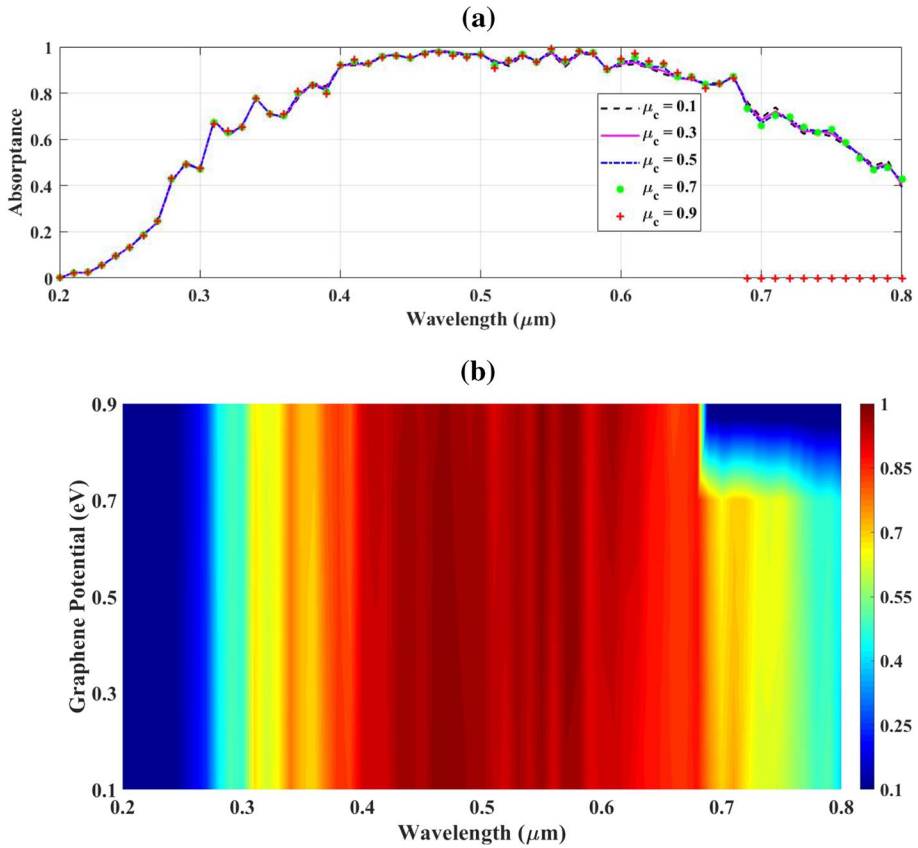


Fig. 6 Absorptance plot for various graphene potential 0.1–0.9 eV for five circle array metasurface design. **a** The line plot represents the absorptance for various values of GCP. The maximum absorptance of 0.993 is achieved at 0.49 μm for GCP value of 0.9 eV, but after 0.69 μm wavelength absorptance value suddenly decreased to near zero value. So, the next best graphene chemical potential value is 0.5 eV which achieves 0.987 absorptance. **b** The plot illustrates that for the values between 0.1 and 0.7 eV there is not much discrepancy with respect to graphene chemical potential. The plot illustrates that the absorptance is highest for 0.4–0.7 μm range. The results are obtained for 0.2–0.8 μm range

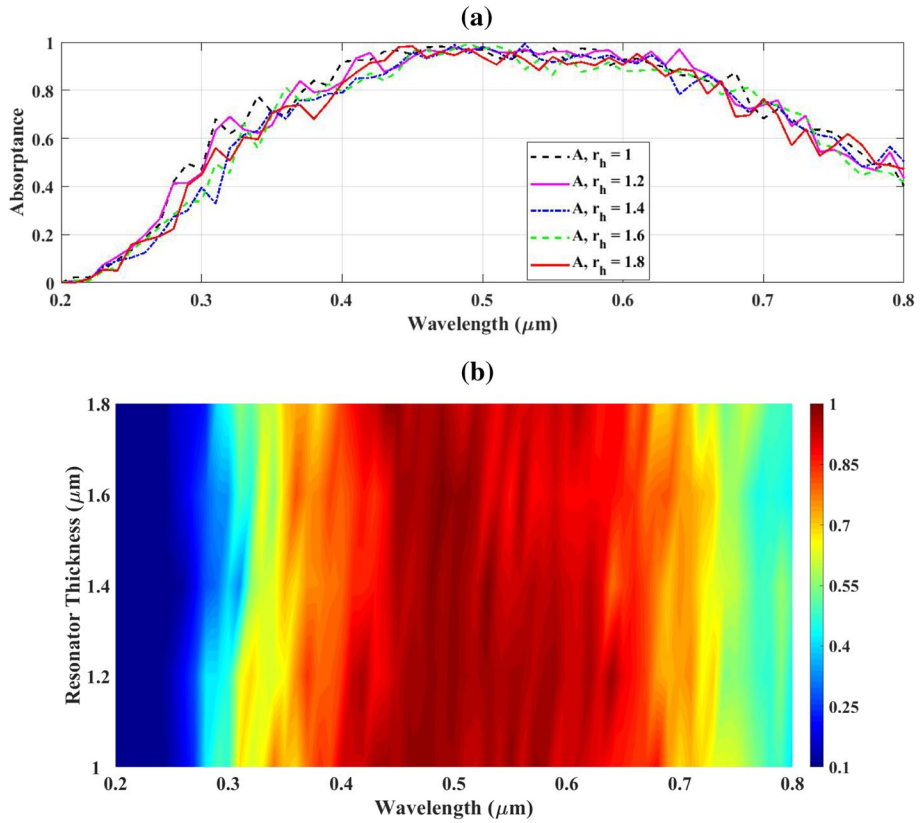


Fig. 7 Absorbance plot for various values of resonator thickness of 1–1.8 μm with the increase in the step of 0.2 μm for five circle array metasurface design. **a** The line plot represents the absorbance for different values of resonator thickness. The maximum absorbance of 0.993 is achieved at 0.49 μm wavelength for resonator thickness of 1.6 μm . **b** The plot illustrates that the absorbance is highest for 0.4–0.7 μm range. The results are obtained for 0.2–0.8 μm range

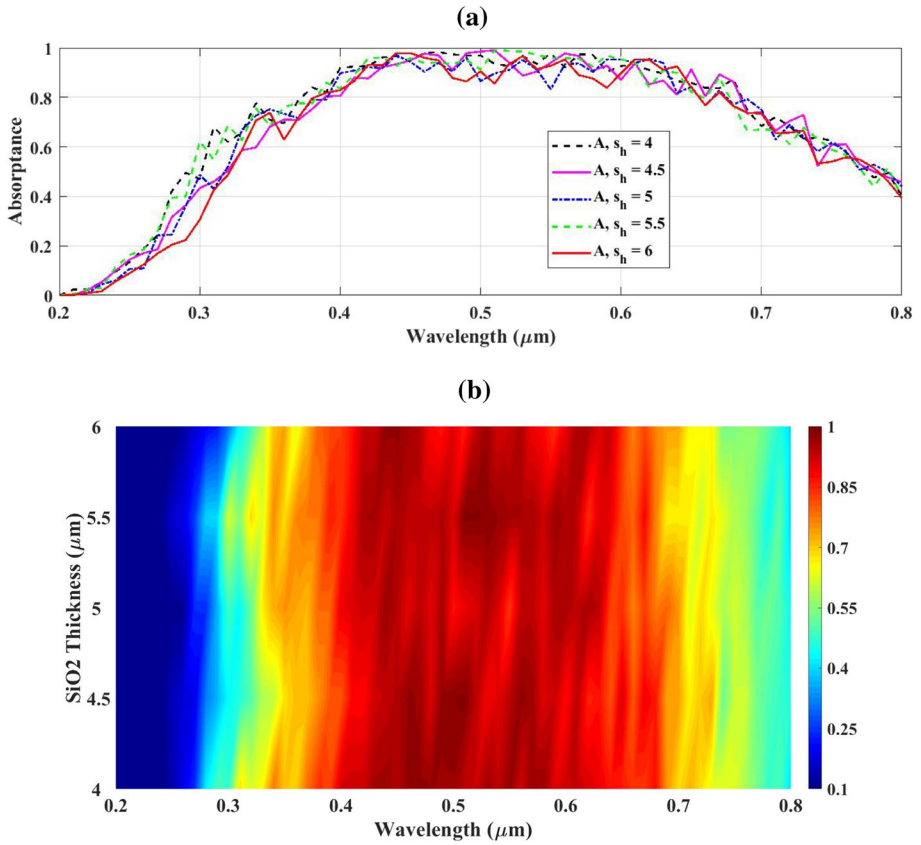


Fig. 8 Absorbance plot for various values of SiO₂ thickness 4–6 μm with the increase in the step of 0.5 μm for five circle array metasurface design. **a** The line plot represents the absorbance for different values of SiO₂ thickness. The maximum absorbance of 0.99 is achieved at 0.49 μm wavelength for SiO₂ thickness of 5.5 μm . **b** The plot illustrates that the absorbance is highest for 0.4–0.7 μm range. The results are obtained for 0.2–0.8 μm range

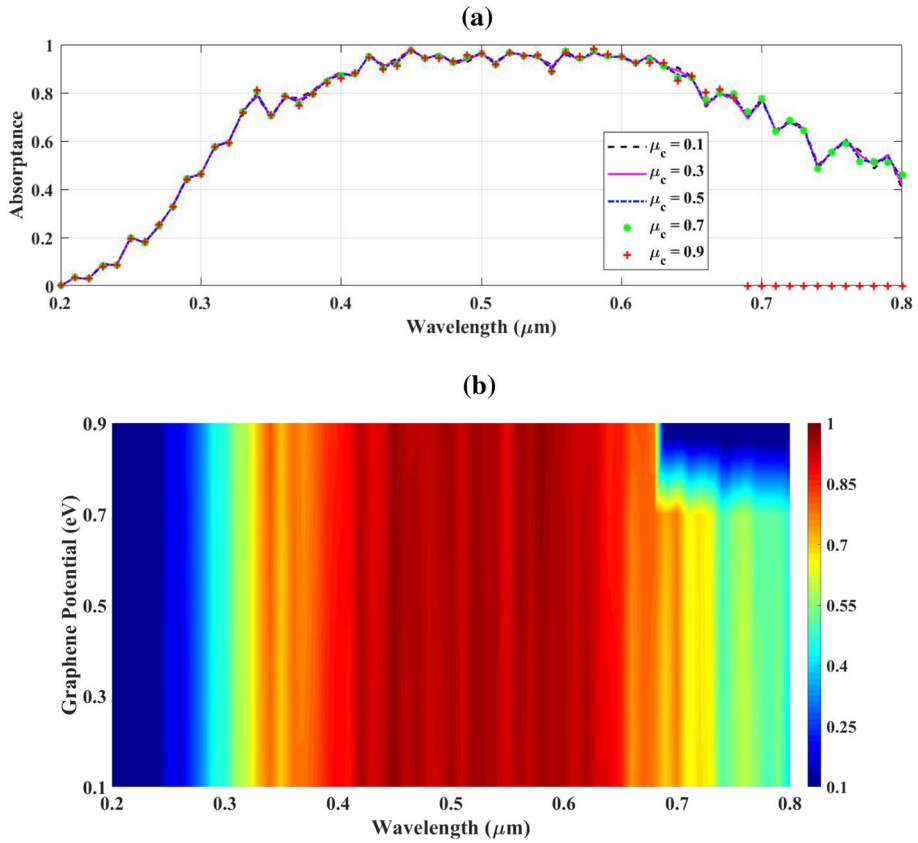


Fig. 9 Absorbance plot for various graphene potential 0.1–0.9 eV for five C-shape array metasurface design. **a** The line plot represents the absorbance for various values of GCP. The maximum absorbance of 0.983 is achieved at 0.58 μm for GCP value of 0.9 eV, but after 0.69 μm wavelength absorbance value suddenly decreased to near zero value. So, the next best graphene chemical potential value is 0.5 eV which achieves 0.987 absorbance. **b** The plot illustrates that for the values between 0.1 and 0.7 eV there is not much discrepancy to GCP. The results are obtained for 0.2–0.8 μm

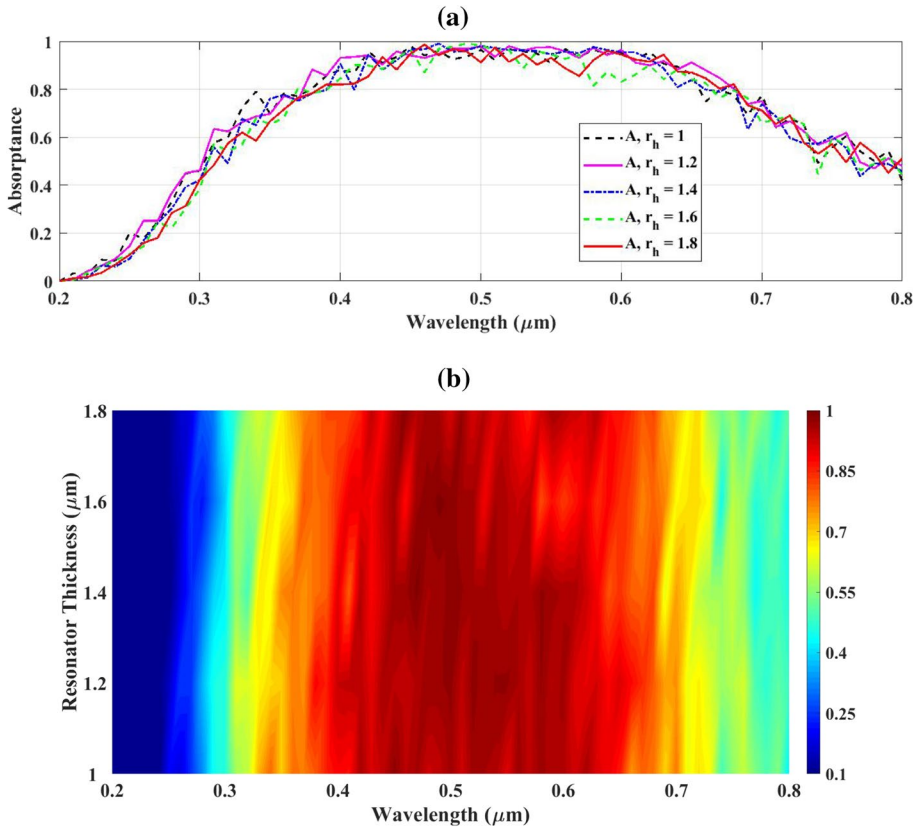


Fig. 10 Absorbance plot for various values of resonator thickness in the range of 1–1.8 μm with the increase in the step of 0.2 μm for five C-shape array metasurface design. **a** The line plot represents the absorbance for different values of resonator thickness. The maximum absorbance of 0.991 is achieved at 0.49 μm wavelength for resonator thickness of 1.6 μm . **b** The plot illustrates that the absorbance is highest for 0.4–0.7 μm range. The results are obtained for 0.2–0.8 μm range

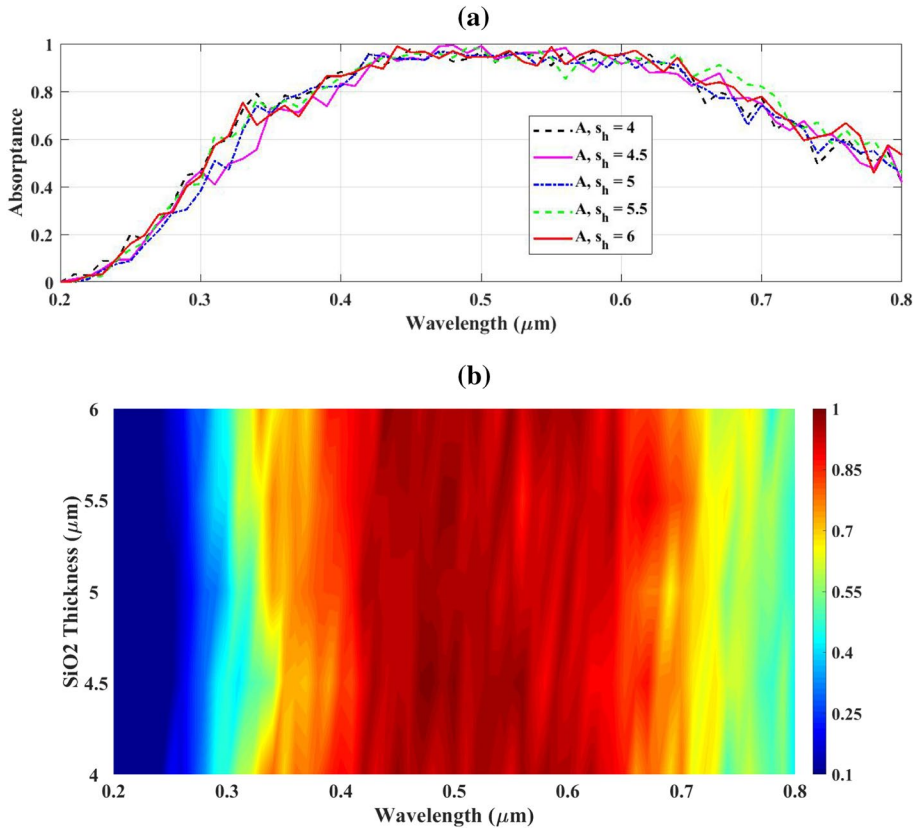


Fig. 11 Absorptance plot for various values of SiO₂ thickness in the range of 4–6 μm with the increase in the step of 0.5 μm for five C-shape array metasurface design. **a** The line plot represents the absorptance for different values of SiO₂ thickness. The maximum absorptance of 0.994 is achieved at 0.49 μm wavelength for SiO₂ thickness of 4.5 μm . **b** The plot illustrates that the absorptance is highest for 0.4–0.7 μm range. The results are obtained for 0.2–0.8 μm range

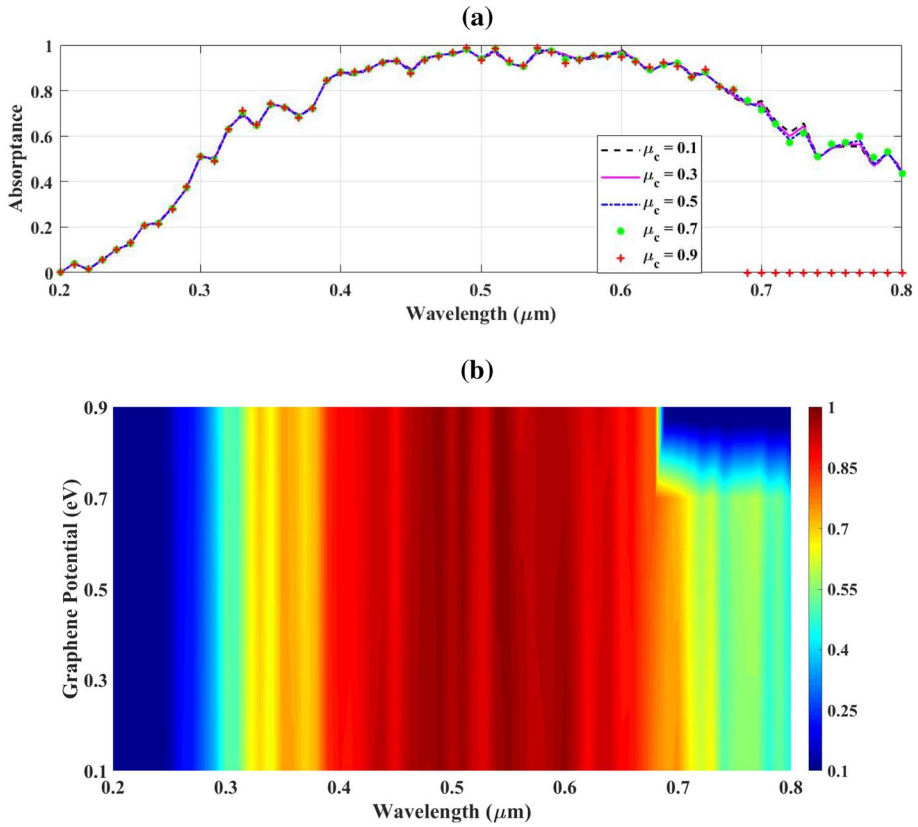


Fig. 12 Absorbance plot for various graphene potential 0.1–0.9 eV for four circle array metasurface design. **a** The line plot represents the absorbance for various values of GCP. The maximum absorbance of 0.987 is achieved at 0.49 μm for GCP value of 0.9 eV, but after 0.69 μm wavelength absorbance value suddenly decreased to near zero value. So, the next best graphene chemical potential value is 0.7 eV which achieves 0.984 absorbance. **b** The plot illustrates that for the values between 0.1 and 0.7 eV there is not much discrepancy to GCP. The results are obtained for 0.2–0.8 μm range

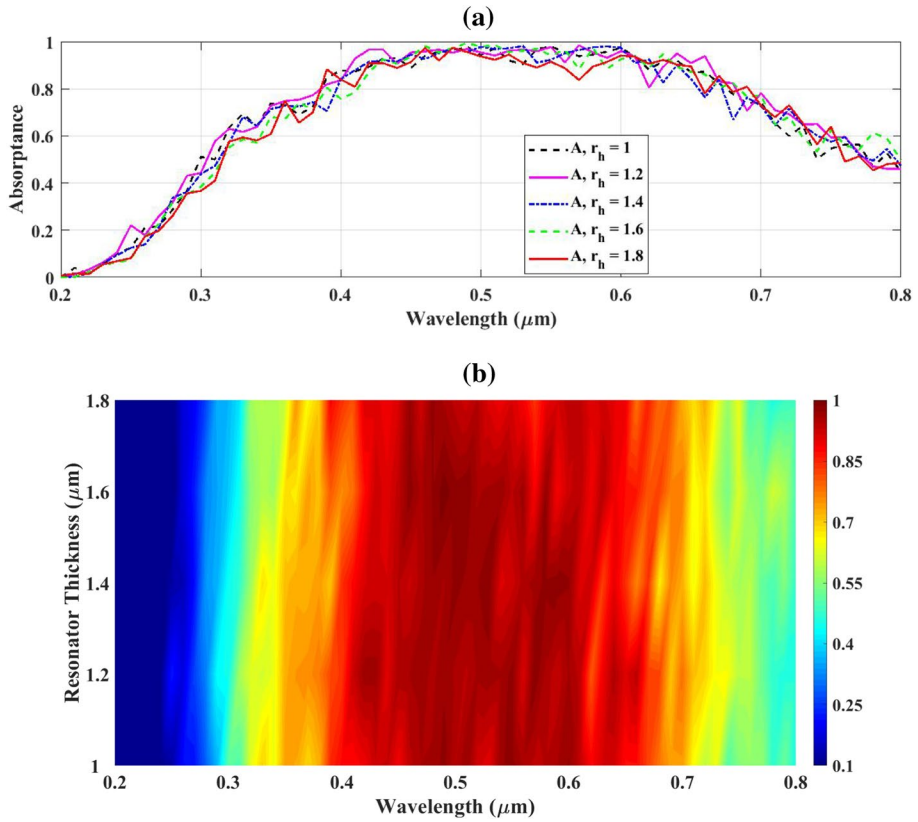


Fig. 13 Absorbance plot for various values of resonator thickness 1–1.8 μm with the increase in the step of 0.2 μm for four circle array metasurface design. **a** The line plot represents the absorbance for different values of resonator thickness. The maximum absorbance of 0.994 is achieved at 0.49 μm wavelength for resonator thickness of 1.6 μm . **b** The plot illustrates that the absorbance is highest in the wavelength ranging between 0.4 and 0.7 μm . The results are obtained for 0.2–0.8 μm range

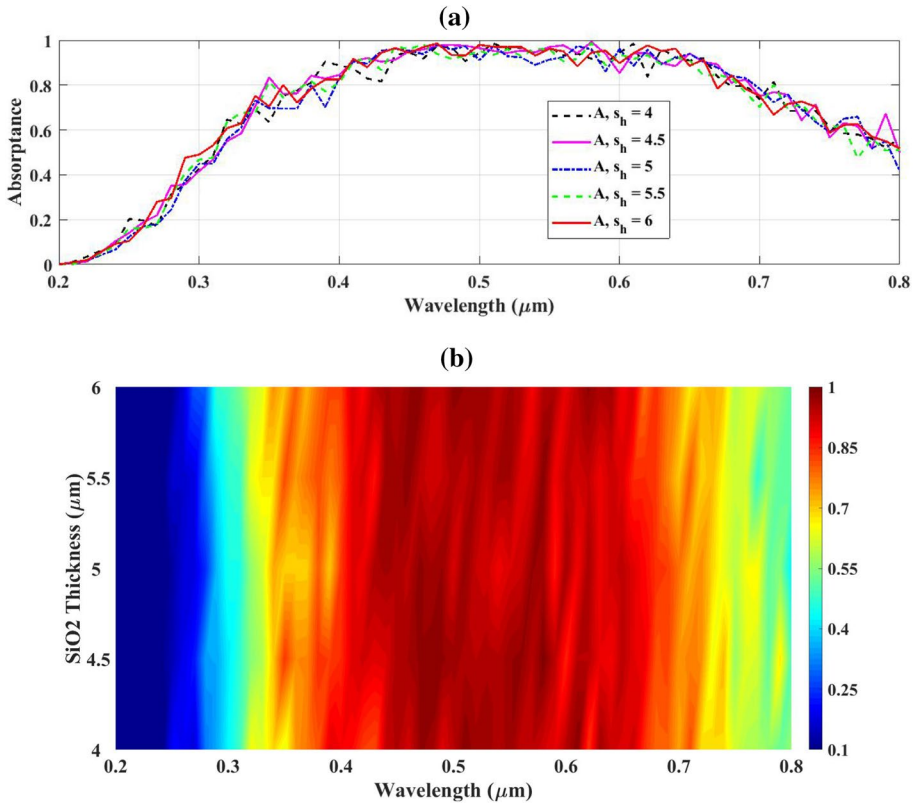


Fig. 14 Absorptance plot for various values of SiO₂ thickness 4–6 μm with the increase in the step of 0.5 μm for four circle array metasurface design. The plot illustrates that the absorptance is highest in the wavelength range of 0.4–0.7 μm . **a** The line plot represents the absorptance for different values of SiO₂ thickness. The maximum absorptance of 0.993 is achieved at 0.49 μm wavelength for SiO₂ thickness of 4.5 μm . **b** The results are obtained for 0.2–0.8 μm range

Table 1 Comparison of four metasurface absorber design

Wavelength range → Design ↓	0.4 to 0.7 μm (Visible region) Average Absorptance (%)
Four C-shape array metasurface absorber design	92
Five circle array metasurface absorber design	91
Five C-shape array metasurface absorber design	90
Four circle array metasurface absorber design	91
Design based on graphene metasurface of Ref. (Charola et al. 2021b)	92
Design based on graphene metasurface of Ref. (Azad et al. 2016)	90
Design based on graphene metasurface of Ref. (Patel et al. 2019)	89.57
C-shaped graphene metasurface-based absorber of Ref. (Patel et al. 2020b)	86.5
Design based on graphene metasurface of Ref. (Liu 2018)	80
Design based on graphene metasurface of Ref. (Sang et al. 2019)	71.1
Design based on graphene metasurface of Ref. (Rufangura and Sabah 2017)	70

Funding The work is supported by start-up and innovation grant under IEDC New Gen project. Department of Science and Technology (DST), Govt. of India, with the Grant No. MU/NewGen/2020/3.

Data availability The data will be made available at a reasonable request to corresponding author.

Declarations

Conflict of interest The authors declare that they have no conflict of interest.

References

- Ahir, P., Patel, S.K., Parmar, J., Katrodiya, D.: Directive and tunable graphene based optical leaky wave radiating structure. *Mater. Res. Express* **6**(5), 055607 (2019). <https://doi.org/10.1088/2053-1591/ab06df>
- Ahmadiwand, A., Gerislioglu, B., Ahuja, R., Kumar Mishra, Y.: Terahertz plasmonics: the rise of toroidal metadevices towards immunobiosensings. *Mater. Today* **32**, 108–130 (2020). <https://doi.org/10.1016/j.mattod.2019.08.002>
- Al-Ashi, N.E., Taya, S.A., El-Naggar, S.A., Vigneswaran, D., Amiri, I.S.: Optical fiber surrounded by a graphene layer as an optical sensor. *Opt. Quant. Electron.* **52**(3), 1–10 (2020). <https://doi.org/10.1007/s11082-020-02288-7>
- Azad, A.K., et al.: Metasurface broadband solar absorber. *Sci. Rep.* **6**(1), 1–6 (2016). <https://doi.org/10.1038/srep20347>
- Bhattacharyya, S., Ghosh, S., Chaurasiya, D., Srivastava, K.V.: Bandwidth-enhanced dual-band dual-layer polarization-independent ultra-thin metamaterial absorber. *Appl. Phys. A Mater. Sci. Process.* **118**(1), 207–215 (2015). <https://doi.org/10.1007/s00339-014-8908-z>
- Charola, S., Patel, S.K., Parmar, J., Jadeja, R.: Multiband Jerusalem cross-shaped angle insensitive metasurface absorber for X-band application. *J. Electromagn. Waves Appl.* (2021a). <https://doi.org/10.1080/09205071.2021.1960643>
- Charola, S., Patel, S.K., Dalsaniya, K., Jadeja, R., Nguyen, T.K., Dhasarathan, V.: Numerical investigation of wideband L-shaped metasurface based solar absorber for visible and ultraviolet region. *Phys. B Condens. Matter* **601**, 412503 (2021b). <https://doi.org/10.1016/j.physb.2020.412503>

- Cheng, Y.Z., Wang, Y., Nie, Y., Gong, R.Z., Xiong, X., Wang, X.: Design, fabrication and measurement of a broadband polarization-insensitive metamaterial absorber based on lumped elements. *J. Appl. Phys.* **111**(4), 044902 (2012). <https://doi.org/10.1063/1.3684553>
- Chou, J.C., et al.: The fabrication and sensing characteristics of arrayed flexible IGZO/Al Urea biosensor modified by graphene oxide. *IEEE Trans. Nanotechnol.* **16**(6), 958–964 (2017). <https://doi.org/10.1109/TNANO.2017.2734894>
- El-Amassi, D.M., Taya, S.A.: Reflection through a parallel-plate waveguide formed by two graphene sheets. *Photon. Nanostruct. Fundam. Appl.* **24**, 53–57 (2017). <https://doi.org/10.1016/j.photonics.2017.03.008>
- Ertürk, G., Özen, H., Tümer, M.A., Mattiasson, B., Denizli, A.: Microcontact imprinting based surface plasmon resonance (SPR) biosensor for real-time and ultrasensitive detection of prostate specific antigen (PSA) from clinical samples. *Sens. Actuat. B Chem.* **224**, 823–832 (2016). <https://doi.org/10.1016/j.snb.2015.10.093>
- Feng, R., Qiu, J., Cao, Y., Liu, L., Ding, W., Chen, L.: Omnidirectional and polarization insensitive nearly perfect absorber in one dimensional meta-structure. *Appl. Phys. Lett.* **105**(18), 181102 (2014). <https://doi.org/10.1063/1.4901073>
- Freise, A.: Optical metamaterials: fundamentals and applications, by W. Cai and V. Shalaev. *Contemp. Phys.* **53**(3), 278–279 (2012). <https://doi.org/10.1080/00107514.2012.661780>
- Gao, R., Xu, Z., Ding, C., Wu, L., Yao, J.: Graphene metamaterial for multiband and broadband terahertz absorber. *Opt. Commun.* **356**, 400–404 (2015). <https://doi.org/10.1016/j.optcom.2015.08.023>
- Geim, A.K., Novoselov, K.S.: The rise of graphene. *Nat. Mater.* (2007). <https://doi.org/10.1038/nmat1849>
- Gerislioglu, B., Dong, L., Ahmadvand, A., Hu, H., Nordlander, P., Halas, N.J.: Monolithic metal dimer-on-film structure: new plasmonic properties introduced by the underlying metal. *Nano Lett.* **20**(3), 2087–2093 (2020). <https://doi.org/10.1021/acs.nanolett.0c00075>
- Guo, W., Liu, Y., Han, T.: Ultra-broadband infrared metasurface absorber. *Opt. Express* **24**(18), 20586–20592 (2016). <https://doi.org/10.1364/oe.24.020586>
- Hanson, G.W.: Dyadic Green's functions and guided surface waves for a surface conductivity model of graphene. *J. Appl. Phys.* **103**(6), 064302 (2008). <https://doi.org/10.1063/1.2891452>
- Landy, N.I., Sajuyigbe, S., Mock, J.J., Smith, D.R., Padilla, W.J.: Perfect metamaterial absorber. *Phys. Rev. Lett.* (2008). <https://doi.org/10.1103/PhysRevLett.100.207402>
- Lenert, A., et al.: A nanophotonic solar thermophotovoltaic device. *Nat. Nanotechnol.* **9**(2), 126–130 (2014). <https://doi.org/10.1038/nnano.2013.286>
- Li, B.X., et al.: Sensing application in fano resonance with T-shape structure. *J. Light. Technol.* **34**(14), 3342–3347 (2016). <https://doi.org/10.1109/JLT.2016.2572723>
- Liu, Y., Liu, Y., Wang, M.: Design, optimization and application of small molecule biosensor in metabolic engineering. *Front. Microbiol.* (2017). <https://doi.org/10.3389/fmicb.2017.02012>
- Liu, B., et al.: Multiband and Broadband Absorption Enhancement of Monolayer Graphene at Optical Frequencies from Multiple Magnetic Dipole Resonances in Metamaterials. *Nanoscale Res. Lett.* (2018). <https://doi.org/10.1186/s11671-018-2569-3>
- Parmar, J., Patel, S.K.: Tunable and highly sensitive graphene-based biosensor with circle/split ring resonator metasurface for sensing hemoglobin/urine biomolecules. *Phys. B Condens. Matter* **624**, 413399 (2021). <https://doi.org/10.1016/j.physb.2021.413399>
- Parmar, J., Patel, S.K., Katrodiya, D., Nguyen, T.K., Skibina, J.S., Dhasarathan, V.: Numerical investigation of gold metasurface based broadband near-infrared and near-visible solar absorber. *Phys. B Condens. Matter* **591**, 412248 (2020). <https://doi.org/10.1016/j.physb.2020.412248>
- Patel, S.K., Parmar, J.: Highly sensitive and tunable refractive index biosensor based on phase change material. *Phys. B Condens. Matter* **622**, 413357 (2021). <https://doi.org/10.1016/j.physb.2021.413357>
- Patel, S.K., Charola, S., Jani, C., Ladumor, M., Parmar, J., Guo, T.: Graphene-based highly efficient and broadband solar absorber. *Opt. Mater. (amst)* (2019). <https://doi.org/10.1016/j.optmat.2019.109330>
- Patel, S.K., Parmar, J., Ladumor, M., Ahmed, K., Nguyen, T.K., Dhasarathan, V.: Numerical simulation of a highly directional optical leaky wave antenna using diamond-shaped graphene perturbations. *Appl. Opt.* **59**(8), 2225–2230 (2020a). <https://doi.org/10.1364/ao.386899>
- Patel, S.K., Charola, S., Parmar, J., Ladumor, M., Ngo, Q.M., Dhasarathan, V.: Broadband and efficient graphene solar absorber using periodical array of C-shaped metasurface. *Opt. Quant. Electron.* **52**(5), 1–19 (2020b). <https://doi.org/10.1007/s11082-020-02379-5>
- Patel, S.K., Parmar, J., Zakaria, R.B., Nguyen, S.A.T.K., Dhasarathan, V.: Sensitivity analysis of metasurface array-based refractive index biosensors. *IEEE Sens. J.* **21**(2), 1470–1477 (2021). <https://doi.org/10.1109/JSEN.2020.3017938>

- Rhee, J.Y., Yoo, Y.J., Kim, K.W., Kim, Y.J., Lee, Y.P.: Metamaterial-based perfect absorbers. *J. Electromagn. Waves Appl.* **28**, 1541–1580 (2014). <https://doi.org/10.1080/09205071.2014.944273>
- Rufangura, P., Sabah, C.: Graphene-based wideband metamaterial absorber for solar cells application. *J. Nanophoton.* **11**(3), 36008 (2017). <https://doi.org/10.1117/1.jnp.11.036008>
- Sang, T., Gao, J., Yin, X., Qi, H., Wang, L., Jiao, H.: Angle-insensitive broadband absorption enhancement of graphene using a multi-grooved metasurface. *Nanoscale Res. Lett* (2019). <https://doi.org/10.1186/s11671-019-2937-7>
- Shelby, R.A., Smith, D.R., Schultz, S.: Experimental verification of a negative index of refraction. *Science* **292**(5514), 77–79 (2001). <https://doi.org/10.1126/science.1058847>
- Shen, Y., Pei, Z., Pang, Y., Wang, J., Zhang, A., Qu, S.: An extremely wideband and lightweight metamaterial absorber. *J. Appl. Phys.* **117**(22), 224503 (2015). <https://doi.org/10.1063/1.4922421>
- Shetti, N.P., Bukkittar, S.D., Reddy, K.R., Reddy, C.V., Aminabhavi, T.M.: Nanostructured titanium oxide hybrids-based electrochemical biosensors for healthcare applications. *Colloids Surf. B* **178**, 385–394 (2019). <https://doi.org/10.1016/j.colsurfb.2019.03.013>
- Shi, X., Zhang, X., Yao, Q., He, F.: A novel method for the rapid detection of microbes in blood using pleurocidin antimicrobial peptide functionalized piezoelectric sensor. *J. Microbiol. Methods* **133**, 69–75 (2017). <https://doi.org/10.1016/j.mimet.2016.12.005>
- Smith, D.R., Padilla, W.J., Vier, D.C., Nemat-Nasser, S.C., Schultz, S.: Composite medium with simultaneously negative permeability and permittivity. *Phys. Rev. Lett.* **84**(18), 4184–4187 (2000). <https://doi.org/10.1103/PhysRevLett.84.4184>
- Son, K.A., Yang, B., Seo, H.C., Wong, D., Moon, J.S., Hussain, T.: High-speed graphene field effect transistors on microbial cellulose biomembrane. *IEEE Trans. Nanotechnol.* **16**(2), 239–244 (2017). <https://doi.org/10.1109/TNANO.2017.2658443>
- Taya, S.A.: P-polarized surface waves in a slab waveguide with left-handed material for sensing applications. *J. Magn. Magn. Mater.* **377**, 281–285 (2015a). <https://doi.org/10.1016/j.jmmm.2014.10.126>
- Taya, S.A.: Theoretical investigation of slab waveguide sensor using anisotropic metamaterial. *Opt. Appl.* **45**(3), 405–417 (2015b). <https://doi.org/10.5277/oa150312>
- Taya, S.A.: Dispersion properties of lossy, dispersive, and anisotropic left-handed material slab waveguide. *Optik (stuttg)* **126**(14), 1319–1323 (2015c). <https://doi.org/10.1016/j.ijleo.2015.04.013>
- Taya, S.A.: Ternary photonic crystal with left-handed material layer for refractometric application. *Opto-Electron. Rev.* **26**(3), 236–241 (2018). <https://doi.org/10.1016/j.opelre.2018.05.002>
- Wang, L., Zhang, Y., Wu, A., Wei, G.: Designed graphene-peptide nanocomposites for biosensor applications: a review. *Anal. Chim. Acta* **985**, 24–40 (2017). <https://doi.org/10.1016/j.aca.2017.06.054>
- Wang, F., Huang, S., Li, L., Chen, W., Xie, Z.: Dual-band tunable perfect metamaterial absorber based on graphene. *Appl. Opt.* (2018). <https://doi.org/10.1364/ao.57.006916>
- Watts, C.M., Liu, X., Padilla, W.J.: Metamaterial electromagnetic wave absorbers. *Adv. Mater.* **24**(23), OP98–OP120 (2012). <https://doi.org/10.1002/adma.201200674>
- Yu, S.G., Yi, W.: Single-walled carbon nanotubes as a chemical sensor for so₂ detection. *IEEE Trans. Nanotechnol.* **6**(5), 545–548 (2007). <https://doi.org/10.1109/TNANO.2007.903800>
- Zhao, X., et al.: Plasmon-exciton coupling by hybrids between graphene and gold nanorods vertical array for sensor. *Appl. Mater. Today* **14**, 166–174 (2019). <https://doi.org/10.1016/j.apmt.2018.12.013>
- Zhong, M.: Design and realization of a perfect metamaterial absorber in terahertz band. *Plasmonics* **15**, 1–8 (2020). <https://doi.org/10.1007/s11468-020-01211-w>

Publisher's Note Springer Nature remains neutral with regard to jurisdictional claims in published maps and institutional affiliations.